ELSEVIER

Comput. Methods Appl. Mech. Engrg. 188 (2000) 413–430

Computer methods in applied mechanics and engineering

www.elsevier.com/locate/cma

Non-Darcy natural convection in a hydrodynamically and thermally anisotropic porous medium

P. Nithiarasu [a,*], K.S. Sujatha [b], K. Ravindran [a], T. Sundararajan [c], K.N. Seetharamu [d]

[a] *Institute for Numerical Methods in Engineering, University of Wales Swansea, Singleton Park, Swansea SA2 8PP, UK*
[b] *Institute of Non-Newtonian Fluid Mechanics, University of Wales Swansea, Singleton Park, Swansea SA2 8PP, UK*
[c] *Department of Mechanical Engineering, Indian Institute of Technology, Chennai 600 036, India*
[d] *School of Mechanical Engineering, Universiti Sains Malaysia, 31750 Tronoh, Malaysia*

Received 21 September 1998

Abstract

The natural convective flow and heat transfer in a fluid saturated anisotropic porous medium have been investigated using the generalised non-Darcy model. A semi-implicit, Galerkin, velocity correction procedure has been employed to solve the governing partial differential equations. Numerical results are presented for different inclinations of the principal permeability directions, Rayleigh and Darcy numbers and permeability and thermal conductivity ratios. The comparison of present results with existing analytical and numerical results shows that present formulation is accurate. A parametric study has been carried out and the difference between the Brinkman and the generalised porous medium models in the context of anisotropic flow is discussed. Significant difference between these models is noticed at higher Rayleigh and Darcy numbers. © 2000 Elsevier Science S.A. All rights reserved.

Keywords: Anisotropic medium; Non-Darcy model; Convection; Semi-implicit time marching; Finite element method

Nomenclature

A	aspect ratio (H/L)
COEFF	coefficient (Eq. (17))
c_p	specific heat
Da	Darcy number (κ_1/L^2)
g	acceleration due to gravity
H	height of the cavity
J	viscosity ratio (μ_{eff}/μ_f)
$\boldsymbol{k}$	thermal conductivity tensor (Eq. (10))
l	length
k_1^* k_2^*	thermal conductivity ratios (Eq. (11))
L	characteristic dimension (width of the cavity, Fig. 1)
$\boldsymbol{M}$	mass matrix (Eq. (16))
$\boldsymbol{N}$	shape functions
Nu	Nusselt number ($=\frac{1}{l}\int_0^l(\partial u/\partial x_1)\,dx_1$ – isothermal vertical walls Eq. (19) – heat flux boundaries)
p	pressure

* Corresponding author. Fax: +0044-01792-29-5676.
E-mail address: p.nithiarasu@swansea.ac.uk (P. Nithiarasu).

0045-7825/00/$ - see front matter © 2000 Elsevier Science S.A. All rights reserved.
PII: S0045-7825(99)00163-2

Pr	Prandtl number (Eq. (4))
q	heat flux
Ra	Rayleigh number (Eqs. (4) and (5))
Ra^*	Darcy–Rayleigh number ($=$Ra Da)
T	temperature
t	time
$\lvert\overline{V}\rvert$	magnitude of velocity vector ($\sqrt{u^2+v^2}$)
u_i, u_j	velocity components
x_i, x_j	coordinate axes

Subscripts

c	cold or center
f	fluid
eff	effective
h	hot
max	maximum
min	minimum
s	solid

Superscripts

n	previous time level
$*$	intermediate velocity components

Greek symbols

α	thermal diffusivity (Eq. (4))
β	coefficient of thermal expansion
ϵ	porosity
γ_i	vector; unity in vertical direction; 0 in horizontal direction
$\boldsymbol{\kappa}$	permeability tensor (Eq. (7))
κ_1, κ_2	principal permeability values
μ	dynamic viscosity
ν	kinematic viscosity
ψ	stream function
σ	ratio of heat capacities, $(\epsilon\ (\rho\ c_p)_f + (1-\epsilon\ (\rho\ c_p)_s)/(\rho\ c_p)_f)$
θ	direction of principal permeabilities
ρ	density

1. Introduction

The natural convection in an anisotropic porous medium is an important area of research due to its wide range of applications including thermal insulation, flow in mushy region of a solidifying alloy [1], flow past heat exchanger tubes [2], etc. Although convection in anisotropic porous media is modelled by many authors, they are not general enough in the sense of the model used and the way in which directional properties are handled. In many of these studies, the principal directions are assumed to coincide with the coordinate axes. With these formulations, influences of the principal directions of the permeability and thermal conductivity upon flow and heat transfer cannot be investigated. Thus we need a generalised procedure and suitable numerical algorithm to solve flow and heat transfer in an anisotropic porous medium.

Based on the Happel and Kuwabara flow models, Neale [3] correlated the anisotropies of flow/diffusion phenomena with medium porosity. Kvernvold and Tyvand [4] have investigated thermal convection in anisotropic porous medium applicable to insulation systems. Ni and Beckermann [5] considered the influence of anisotropic property ratios upon the natural convective heat transfer in a square cavity filled with fluid saturated anisotropic porous media. Thermal convection has been analysed by Chang and Lin [6] in a

square cavity with finite wall thickness and convection in a cylinder filled with anisotropic porous medium has been investigated by Chang and Haiso [7]. Recently, Degan et al. [8] studied the effects of principal permeability directions and the influence of permeability and conductivity ratios on natural convective heat transfer. Their analysis predicts that the maximum heat transfer occurs when the principal permeability directions are oriented in the direction of coordinate axes, with a higher permeability in the flow direction. Several studies have been reported in literature on natural convective heat transfer in enclosures heated from below. For instance, Epherre [9], Castinel and Combarnous [10], McKibbin and Tyvand [11], Gjerde and Tyvand [12] Nilsen and Storesletten [13] are few of them.

These available studies on convection in anisotropic porous medium use Darcy's model which is limited to well packed and low permeability media. Industrial applications such as flow over tube bundles (as in nuclear reactor core) and solidification of metal alloys demand a non-Darcian approach which suitably accounts porosity in addition to the non-Darcian forces such as viscous and drag effects. Although many studies are available on generalised non-Darcian natural convection in enclosures for isotropic porous media [14–20] the generalised approach to flow in anisotropic porous media is not available.

There are few recent studies which use formulations in terms of principal values of properties and its orientations [8,21]. However, these studies are again not generalised in terms of the model used. Many features have been ignored in these recent studies. First of all, they are based on either the Darcy or Brinkman models. Earlier study with the generalised model without off-diagonal permeability terms [22] suggests that the parameters such as porosity does have an effect on the results. It is therefore important to formulate the anisotropic porous medium flows using the generalised model due to its wide range of industrial applications. Also, many porous medium flows need to be solved with respect to time to study the impact of flow evolution. It is also important to have a suitable and simple solution procedure to solve the transient porous medium equations. In this paper, we describe the implementation of the velocity correction procedure for a more general hydrodynamically and thermally anisotropic porous medium. Several numerical examples are presented and compared with the existing results. A parametric study is also carried out for different inclination angles, permeability ratios and Darcy and Rayleigh numbers using the present generalised approach and the differences between the Brinkman and the generalised porous medium flow models are quantitatively determined.

2. Problem formulation and governing equations

A hydrodynamically and thermally anisotropic porous medium in an enclosure saturated with a fluid is considered (Fig. 1). All the properties except the density are assumed to be constant. The density variation is incorporated by invoking the Bousenesq approximation for buoyancy driven flows. The generalised governing equations for the porous medium flow in non-dimensional form are (for buoyancy driven flows) [16–20]

Continuity

$$\frac{\partial u_i}{\partial x_i} = 0. \tag{1}$$

Momentum equation

$$\frac{1}{\epsilon}\frac{\partial u_i}{\partial t} + \frac{1}{\epsilon^2} u_j \frac{\partial u_i}{\partial x_j} = -\frac{\partial p}{\partial x_i} + \frac{J\,\mathrm{Pr}}{\epsilon}\left[\frac{\partial^2 u_i}{\partial x_i^2}\right] - \frac{\mathrm{Pr}}{\kappa_{ij}} u_i - \frac{1.75}{\sqrt{150}} \frac{|\overline{V}|}{\sqrt{\kappa_{ij}}} \frac{u_i}{\epsilon^{3/2}} + \gamma_i \mathrm{Ra}\ \mathrm{Pr}\, T. \tag{2}$$

Energy equation

$$\sigma \frac{\partial T}{\partial t} + u_j \frac{\partial T}{\partial x_j} = k_{ij}\left(\frac{\partial^2 T}{\partial x_i^2}\right). \tag{3}$$

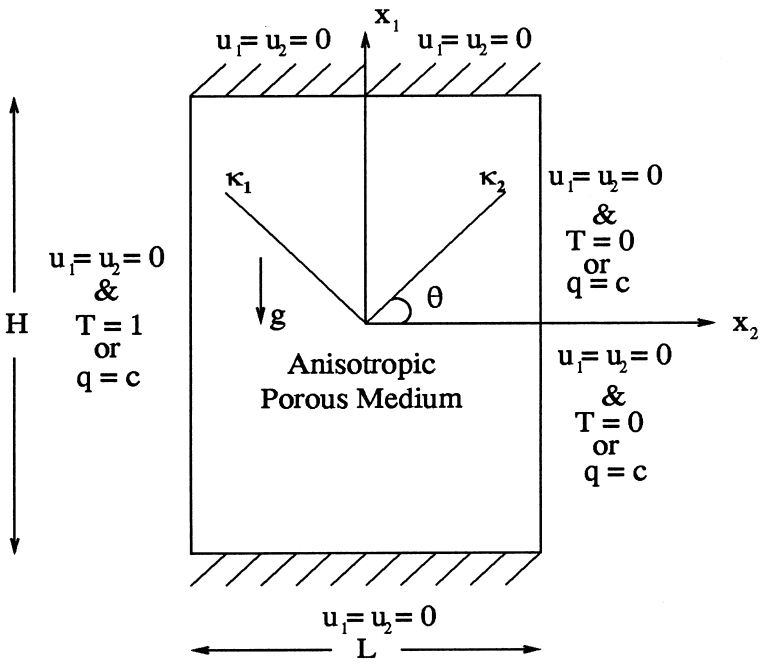

Fig. 1. Buoyancy driven flow in a fluid saturated anisotropic porous medium.

The following scales are used to non-dimensionalise the above equations

$$x_i = \frac{\overline{x}_i}{L}, \quad u_i = \frac{\overline{u}_i L}{\alpha_f}, \quad p = \frac{\overline{p}\alpha_f}{\rho L^2}, \quad t = \frac{\overline{t}\alpha_f}{L^2}, \quad T = \frac{T - T_c}{T_h - T_c},$$
$$\alpha_f = \frac{k_f}{(\rho c_p)_f}, \quad \mathrm{Pr} = \frac{\nu_f}{\alpha_f}, \quad \mathrm{Ra} = \frac{g\beta\Delta T L^3}{\nu_f \alpha_f}, \quad J = \frac{\nu_{eff}}{\nu_f}, \tag{4}$$

where the over-line indicates a dimensional quantity. Above scales are applicable for the differentially heated cavity with isothermal vertical walls. When the enclosure is subjected to constant heat flux, following temperature scale and Rayleigh number definition are used [23]

$$T = \frac{\overline{T} - T_c}{qL/k_f}, \quad \mathrm{Ra} = \frac{g\beta q L^4}{k_f \nu_f \alpha_f}. \tag{5}$$

The detailed derivation of the governing equations are discussed elsewhere [14,16]. In the momentum Eq. (2), the non-linear matrix drag is incorporated through the Ergun's correlation [24]. In the governing equations, u and v are volume averaged velocity components; ϵ the porosity of the medium and is assumed to be uniform throughout the domain in the present study; Pr the Prandtl number (unity in this study); Ra the fluid Rayleigh number; σ the ratio of heat capacities; T the non-dimensional temperature, J the viscosity ratio, (This ratio is taken as unity in the present study for the sake of simplicity.) κ_{ij} and k_{ij} are permeability and thermal conductivity tensors respectively; ν the kinematic viscosity; q the heat flux and α the thermal diffusivity. Subscript f indicates fluid; 'eff' indicates effective; h indicates hot and c indicates cold or center. See Nomenclature for details.

The permeability tensor in the momentum equations is given as [8,21]

$$\overline{\boldsymbol{\kappa}} = \begin{bmatrix} \kappa_1 \cos^2\theta + \kappa_2 \sin^2\theta & (\kappa_1 - \kappa_2)\sin\theta\cos\theta \\ (\kappa_1 - \kappa_2)\sin\theta\cos\theta & \kappa_1 \sin^2\theta + \kappa_2 \cos^2\theta \end{bmatrix}, \tag{6}$$

where κ_1 and κ_2 are the principal permeability values and θ is the angle between κ_2- and x_2-directions (Fig. 1).

Now the inverse, non-dimensional permeability tensor is calculated as

$$[\boldsymbol{\kappa}^{-1}] = \frac{1}{\mathrm{Da}} \begin{bmatrix} \cos^2\theta + \kappa^* \sin^2\theta & (1-\kappa^*)\sin\theta\cos\theta \\ (1-\kappa^*)\sin\theta\cos\theta & \kappa^*\cos^2\theta + \sin^2\theta \end{bmatrix} \tag{7}$$

and the inverse of square root of the permeability tensor is

$$[\sqrt{\boldsymbol{\kappa}}]^{-1} = \frac{1}{\sqrt{\mathrm{Da}}} \begin{bmatrix} \cos^2\theta + \sqrt{\kappa^*}\sin^2\theta & (1-\sqrt{\kappa^*})\sin\theta\cos\theta \\ (1-\sqrt{\kappa^*})\sin\theta\cos\theta & \sqrt{\kappa^*}\cos^2\theta + \sin^2\theta \end{bmatrix}, \tag{8}$$

where

$$\mathrm{Da} = \frac{\kappa_1}{L^2}, \quad \kappa^* = \frac{\kappa_1}{\kappa_2}. \tag{9}$$

The thermal conductivity tensor in its non-dimensional form is given by

$$[\boldsymbol{k}] = \begin{bmatrix} k_1^* & 0 \\ 0 & k_2^* \end{bmatrix}, \tag{10}$$

where

$$k_1^* = \frac{k_1}{k_\mathrm{f}}, \quad k_2^* = \frac{k_2}{k_\mathrm{f}}. \tag{11}$$

In the above relations, Da is the Darcy number, k_1 and k_2 are thermal conductivities in x_1 and x_2 directions, respectively. The off diagonal terms in Eq. (10) are omitted for the sake of simplicity.

In the governing equations (Eqs. (1)–(3)), the complexity is mainly introduced by the anisotropic porous medium terms (linear and non-linear terms). It is therefore necessary to devise a proper solution procedure to handle these terms. To the knowledge of the authors, no literature is available on the solution of generalised anisotropic porous medium equations. It is rather difficult to get any form of analytical solution for these equations discussed above. In the following section, we give the necessary modifications required for an anisotropic medium from an isotropic model proposed earlier [17]. Although the present procedure is an extension of the previous work, it is not straight forward. Here we need to handle the anisotropic terms which contains both the velocity components. Thus treating the whole porous medium terms implicitly as in the previous work [17] is not possible and part of it need to be treated explicitly, which may pose some time step restrictions.

3. Solution procedure and numerical method

The present work differs from the earlier one due to the anisotropy introduced here. Also some differences in splitting the equations have been incorporated for the sake of easy handling. Now the x_1 component of the momentum equation (vertical direction, Fig. 1) can be rewritten as

$$\begin{aligned} &\frac{1}{\epsilon}\frac{\partial u_1}{\partial t} + \frac{1}{\epsilon^2}u_1\frac{\partial u_1}{\partial x_1} + \frac{1}{\epsilon^2}u_2\frac{\partial u_1}{\partial x_2} \\ &\quad = -\frac{\partial p}{\partial x_1} + \frac{J\,\mathrm{Pr}}{\epsilon}\left(\frac{\partial^2 u_1}{\partial x_1^2} + \frac{\partial^2 u_1}{\partial x_2^2}\right) - \frac{\mathrm{Pr}}{\mathrm{Da}}\left[(\cos^2\theta + \kappa^*\sin^2\theta)u_1 + \{(1-\kappa^*)\sin\theta\cos\theta\}u_2\right] \\ &\qquad - \frac{1.75}{\sqrt{150}}\frac{\sqrt{u_1^2+u_2^2}}{\sqrt{\mathrm{Da}}}\left[(\cos^2\theta + \sqrt{\kappa^*}\sin^2\theta)u_1 + \left\{(1-\sqrt{\kappa^*})\sin\theta\cos\theta\right\}u_2\right] + \mathrm{Ra}\ \mathrm{Pr}\,T. \end{aligned} \tag{12}$$

In the absence of anisotropy, all porous medium terms can be treated implicitly [17,18]. However, here, the porous medium terms cannot be handled implicitly due to the appearance of two different components of porous medium terms with two different velocity components. Thus the porous medium terms need to be split into two parts as discussed below.

The Eulerian velocity correction procedure used in this study is well documented in many articles for single phase flows [25–28] and porous medium flows [17,18]. The method can be summarised into following steps

(i) Calculate the intermediate velocity components from the momentum equations after neglecting the pressure term. In the earlier study [17] this step is straight forward and the intermediate velocities can be calculated directly by implicitly treating the porous medium terms. However, in anisotropic porous medium problems, both velocity components are present in both the components of the momentum equations as dependent variables. Thus, when solving x_1 component of the momentum equations, the parts of porous medium terms which contains x_2 component velocity can only be treated explicitly and vise versa.

(ii) Find the pressure field using the intermediate velocity components and the continuity equation (the Poisson equation). Here a pressure Poisson equation derived from the continuity is used [25–28].

(iii) Correct the velocities using the pressure distribution obtained from step (ii) and

(iv) Determine the temperature distribution using the calculated velocity and pressure fields.

The four steps listed above constitute the standard velocity correction procedure followed in most of the available literature. However, a modification in step one can be made to separate the porous medium and other terms (two steps). Thus programming will be systematic and single phase flow can be solved by simply eliminating the porous medium step. To separate the porous terms, we calculate the intermediate velocity components in two steps. In the first step, a velocity field without the porous medium terms is obtained. The true intermediate velocity components are calculated from the porous medium terms in the second step. Now Eq. (12) can be discretized in time as (without pressure term)

$$\frac{1}{\epsilon}\left[\frac{u_1^{**}-u_1^n}{\Delta t}\right] = -\left[\frac{1}{\epsilon^2}u_1\frac{\partial u_1}{\partial x_1}+\frac{1}{\epsilon^2}u_2\frac{\partial u_1}{\partial x_2}\right]^n + \frac{J\,\mathrm{Pr}}{\epsilon}\left(\frac{\partial^2 u_1}{\partial x_1^2}+\frac{\partial^2 u_1}{\partial x_2^2}\right)^n + \mathrm{Ra}\ \mathrm{Pr}\, T^n \tag{13}$$

and

$$\begin{aligned}\frac{1}{\epsilon}\left[\frac{u_1^{*}-u_1^{**}}{\Delta t}\right] = & -\frac{\mathrm{Pr}}{\mathrm{Da}}(\cos^2\theta+\kappa^*\sin^2\theta)u_1^* - \frac{\mathrm{Pr}}{\mathrm{Da}}\{(1-\kappa^*)\sin\theta\cos\theta\}u_2^n \\ & -\frac{1.75}{\sqrt{150}}\frac{\sqrt{(u_1^2+u_2^2)^n}}{\sqrt{\mathrm{Da}}}(\cos^2\theta+\sqrt{\kappa^*}\sin^2\theta)u_1^* \\ & -\frac{1.75}{\sqrt{150}}\frac{\sqrt{(u_1^2+u_2^2)^n}}{\sqrt{\mathrm{Da}}\sqrt{\kappa^*}}\{(1-\sqrt{\kappa^*})\sin\theta\cos\theta\}u_2^n\end{aligned} \tag{14}$$

where u_1^* is the intermediate velocity component in x_1 direction. In the above step (Eq. (14)), it should be noted that the porous medium terms are split into two parts with one treated at $n+1$th time level (terms with superscript *) and the other at nth level (terms with superscript n). The spatial discretization using the Galerkin method to Eq. (13) is straight forward and the mass matrix can be lumped to update the solution [26–28]. Eq. (14) is also discretized in a similar manner and the coefficients of the mass matrix can be collected as

$$\begin{aligned}&\left[\frac{1}{\epsilon}+\frac{\mathrm{Pr}}{\mathrm{Da}}(\cos^2\theta+\kappa^*\sin^2\theta)+\frac{1.75}{\sqrt{150}}\frac{(\sqrt{u_1^2+u_2^2})^n}{\sqrt{\mathrm{Da}}}(\cos^2\theta+\sqrt{\kappa^*}\sin^2\theta)\right][\boldsymbol{M}]\{\overline{\boldsymbol{u}_1^*}\} \\ &\quad=\frac{1}{\epsilon}[\boldsymbol{M}]\{\overline{\boldsymbol{u}_2^{**}}\}-\frac{\mathrm{Pr}}{\mathrm{Da}}(\sqrt{1-\kappa^*})\sin\theta\cos\theta[\boldsymbol{M}]\{\overline{\boldsymbol{u}_2^n}\} \\ &\qquad-\frac{1.75}{\sqrt{150}}\frac{\sqrt{(u_1^2+u_2^2)^n}}{\sqrt{\mathrm{Da}}}(1-\sqrt{\kappa^*})\sin\theta\cos\theta[\boldsymbol{M}]\{\overline{\boldsymbol{u}_2^n}\}\end{aligned} \tag{15}$$

where $[\boldsymbol{M}]$ is the mass matrix given as

$$[\boldsymbol{M}]=\int_\Omega N^{\mathrm{T}}N\,\mathrm{d}\Omega. \tag{16}$$

Substituting

$$\mathrm{COEFF} = \frac{1}{\epsilon} + \frac{\mathrm{Pr}}{\mathrm{Da}}(\cos^2\theta + \kappa^* \sin^2\theta) + \frac{1.75}{\sqrt{150}} \frac{(\sqrt{u_1^2 + v_1^2})^n}{\sqrt{Da}} (\cos^2\theta + \sqrt{\kappa^*} \sin^2\theta) \tag{17}$$

into Eq. (15) and rearranging terms gives

$$[\boldsymbol{M}]\{\overline{\boldsymbol{u}_1^*}\} = \frac{1}{\mathrm{COEFF}} \left\{ \frac{1}{\epsilon} [\boldsymbol{M}]\{\overline{\boldsymbol{u}_1^{**}}\} - \frac{\mathrm{Pr}}{\mathrm{Da}} (1 - \kappa^*) \sin\theta \cos\theta [\boldsymbol{M}]\{\overline{u_2^n}\} \right\}$$

$$- \frac{1}{\mathrm{COEFF}} \left\{ \frac{1.75}{\sqrt{150}} \frac{(\sqrt{u_1^2 + v_1^2})^n}{\sqrt{\mathrm{Da}}} (1 - \sqrt{\kappa^*}) \sin\theta \cos\theta [\boldsymbol{M}]\{\overline{\boldsymbol{u}_2^n}\} \right\}. \tag{18}$$

The mass matrix $[\boldsymbol{M}]$ in the LHS can now be lumped to advance the solution in time by just updating at each time step.

4. Numerical examples and discussion

The buoyancy driven flow in a differentially heated square cavity with isothermal vertical walls is considered as a first problem (Fig. 1), which is a standard benchmark example used by many authors. The natural convection inside the cavity is investigated for different Rayleigh numbers, permeability and thermal conductivity ratios and principal permeability directions. Present predictions are compared with the available results wherever possible.

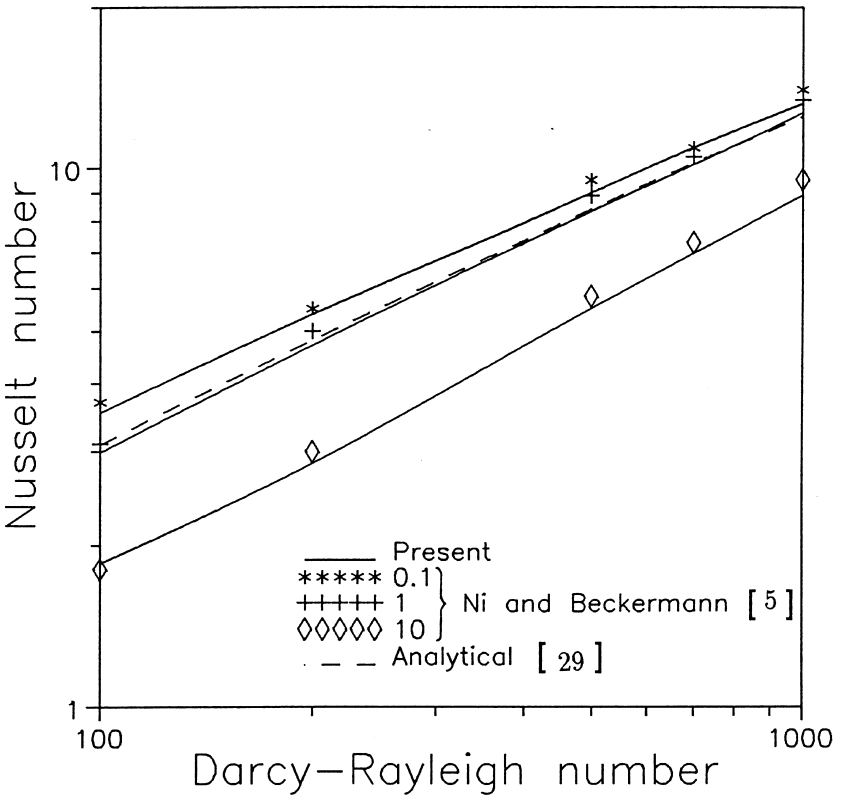

Fig. 2. Average nusselt number variation with Darcy–Rayleigh number for different conductivity ratios, $\mathrm{Da} = 10^{-6}$, $\epsilon = 0.6$, $A = 1$, $\theta = 0°$.

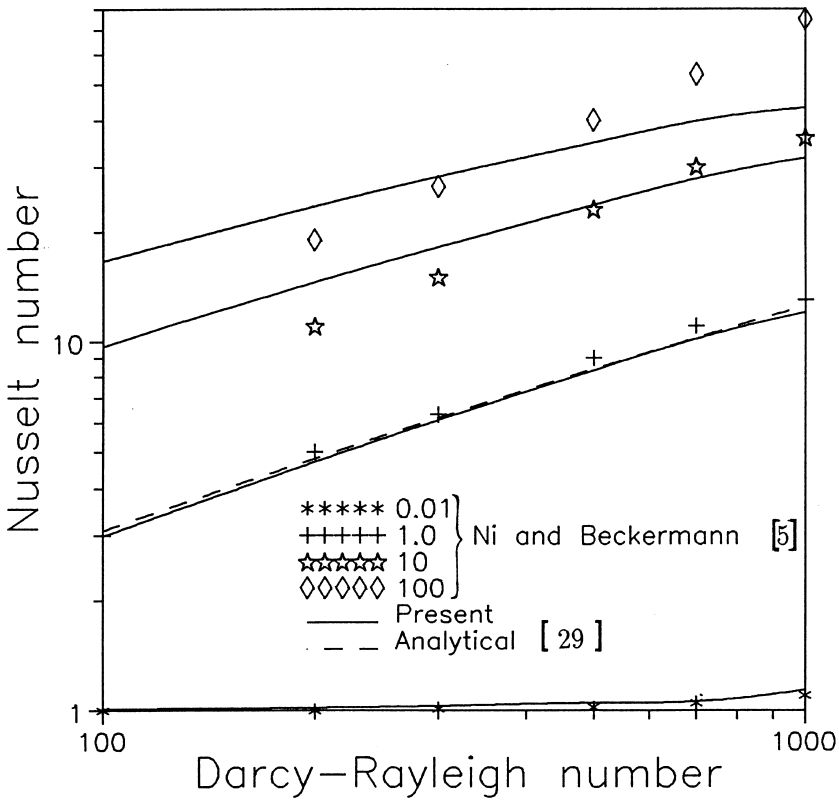

Fig. 3. Average nusselt number variation with Darcy–Rayleigh number for different permeability ratios, $Da = 10^{-6}$, $\epsilon = 0.6$, $A = 1$, $\theta = 0^{\circ}$.

A finite element grid of size 51×51 is used in all the examples considered in this study. The mesh is finely graded near the walls of the enclosure to resolve the boundary layer accurately. The first node from the walls is placed at a non-dimensional distance of 0.005.

From the anisotropic relations, it is possible to find many limiting cases of the porous medium flows by changing the inclination angles of principal permeability directions. For example, at $\theta = 0^{\circ}$ and 90°, the off-diagonal terms of the permeability tensor vanish and the principal directions coincide with the co-ordinate axes. These limiting cases can be compared with the existing results without the off-diagonal terms. Such an exercise is carried out to validate the numerical method and the model. Figs. 2 and 3 show the comparison of the present results with those of available in literature. The referred paper [5] used a different formulation where the Darcy–Rayleigh number (Ra^{*}) is defined based on the principal permeability κ_2. In order to match the available formulation, the present equations are also modified for the sake of comparison. It is seen that the agreement is generally good in the Darcy–Rayleigh number range considered. The differences at higher permeability ratios can be attributed to the Darcy model and uniform grid used in the referred paper [5]. When the permeability ratio is unity, present predictions agree excellently with the analytical solution [29].

Above results are for a limiting case without the off-diagonal permeability values. Further results are obtained for arbitrary variation of θ and are discussed below. Another problem with flux boundary conditions is discussed and compared with the existing results later. The available results on anisotropic porous medium with arbitrary variation of θ and heat flux boundary conditions use the Brinkman extension to the Darcy model [21]. The full generalised model is essential in many applications as mentioned earlier. In this section, therefore, difference between the Brinkman and generalised models is discussed first. Here the results are obtained for different Darcy and Rayleigh numbers and principal permeability directions using both the Brinkman and the generalised models.

Table 1
Comparison of average Nusselt number predictions between the Brinkman and the generalised porous medium models in the Darcy flow regime, Da $= 10^{-6}$

Sl. No.	θ	κ^*	Ra	Nu	
				Brinkman	General
1	0°	0.1	10^8	3.792	3.737
2	45°	0.1	10^8	4.529	4.507
3	90°	0.1	10^8	9.357	9.385
4	0°	10	10^8	2.692	2.741
5	45°	10	10^8	1.291	1.288
6	90°	10	10^8	1.118	1.097
7	0°	0.1	10^9	13.836	13.505
8	45°	0.1	10^9	18.865	17.938
9	90°	0.1	10^9	33.596	28.353
10	0°	10	10^9	11.970	11.490
11	45°	10	10^9	4.119	4.155
12	90°	10	10^9	3.253	3.422

Table 2
Comparison of average Nusselt number predictions between the Brinkman and the generalised porous medium models in the non-Darcy flow regime, Da $= 10^{-2}$

Sl. No.	θ	κ^*	Ra	Nu	
				Brinkman	General
1	0°	0.1	10^4	1.892	1.587
2	45°	0.1	10^4	1.870	1.573
3	90°	0.1	10^4	1.891	1.579
4	0°	10	10^4	1.140	1.106
5	45°	10	10^4	1.153	1.119
6	90°	10	10^4	1.141	1.106
7	0°	0.1	10^5	4.393	3.475
8	45°	0.1	10^5	4.425	3.456
9	90°	0.1	10^5	4.491	3.499
10	0°	10	10^5	3.203	2.761
11	45°	10	10^5	3.191	2.853
12	90°	10	10^5	2.951	2.636

Tables 1 and 2 show the average Nusselt number predictions in Darcy and non-Darcy flow regimes respectively for different Rayleigh numbers, permeability ratios and θ values. In both the tables the average Nusselt numbers predicted from both the Brinkman and generalised models are presented. In the Darcy flow regime (Da $= 10^{-6}$, Table 1), the Nusselt numbers predicted by the generalised model are smaller than that of the Brinkman model. This under prediction by the generalised model can be attributed to the inclusion of non-linear and porosity effects. The difference is higher at higher Rayleigh numbers and smaller permeability ratios. A maximum difference of about 18% has been observed at Ra $= 10^9$.

In Table 2, the non-Darcy flow regime results are presented. At a Darcy number of 10^{-2}, the non-Darcian forces will be much higher than that of the Darcy regime considered earlier. Here the Darcy model and extensions to the Darcy model can not predict accurate results. It is clear from Table 2 that the generalised model predicts a much lower Nusselt number than that of Brinkman model for the given parameters. Especially at higher Rayleigh numbers, the non-linear effects strongly influence the Nusselt number predictions. A maximum difference in Nusselt number of about 28% is observed between the two models. This shows the influence of the non-linear terms included in the present generalised model.

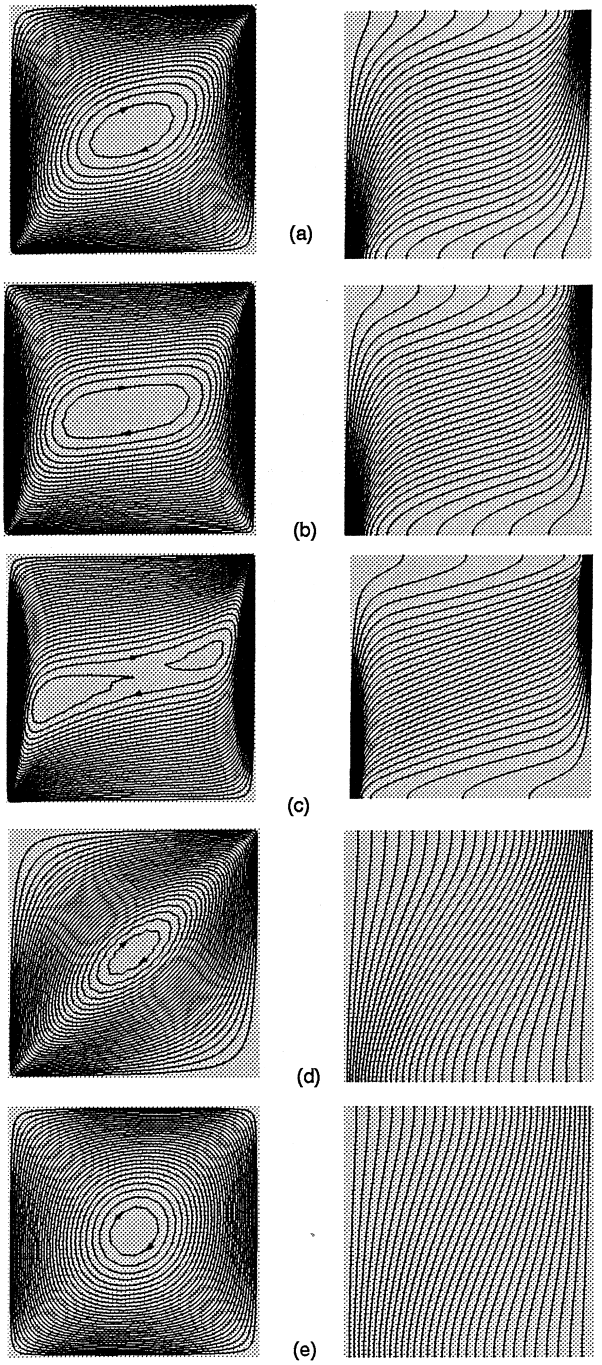

Fig. 4. Flow and isotherm patterns for different θ and permeability ratios in the Darcy flow regime, $Da = 10^{-6}$, $Ra = 10^{8}$, $\epsilon = 0.5$, $k_1^* = 1$, $k_2^* = 1$: (a) $\kappa^* = 0.1$, $\theta = 0°$, $\psi_{max} = 6.041$; (b) $\kappa^* = 0.1$, $\theta = 45°$, $\psi_{max} = 6.154$; (c) $\kappa^* = 0.1$, $\theta = 90°$, $\psi_{max} = 13.741$; (d) $\kappa^* = 10$, $\theta = 45°$, $\psi_{max} = 1.666$; (e) $\kappa^* = 10$, $\theta = 90°$, $\psi_{max} = 0.804$.

In Figs. 4–7, a detail account of flow and isotherm patterns for different Darcy and Rayleigh numbers, θ and permeability ratios have been presented using the generalised model. In the Darcy flow regime ($Da = 10^{-6}$), the thermal and momentum boundary layers become thinner with increase in θ values for a permeability ratio of 0.1 and Rayleigh number of 10^8 (Fig. 4(a)–(c)). This is an indication of higher energy transfer between the cold and hot walls with increase in θ. As the principal permeability κ_1 is assumed to be

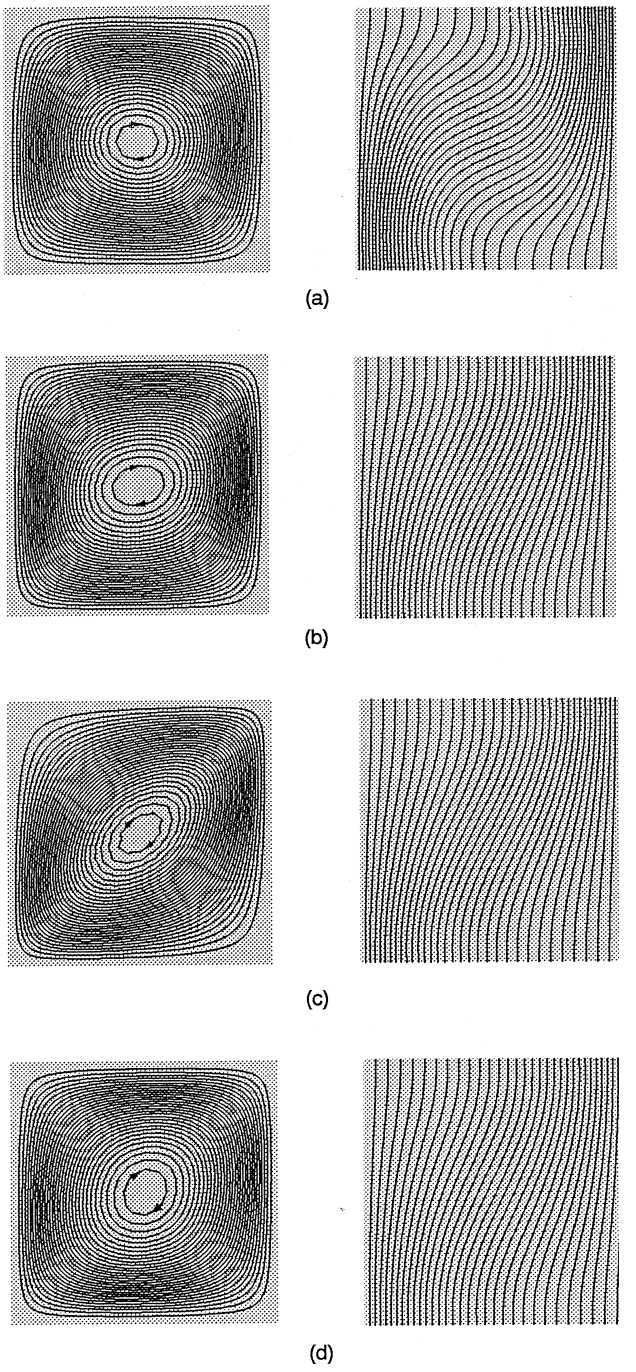

Fig. 5. Flow and isotherm patterns for different θ and permeability ratios in the non-Darcy flow regime, $Da = 10^{-2}$, $Ra = 10^4$, $\epsilon = 0.5$, $k_1^* = 1$, $k_2^* = 1$: (a) $\kappa^* = 0.1$, $\theta = 45°$, $\psi_{max} = 2.766$; (b) $\kappa^* = 10$, $\theta = 0°$, $\psi_{max} = 0.933$; (c) $\kappa^* = 10$, $\theta = 45°$, $\psi_{max} = 1.117$; (d) $\kappa^* = 10$, $\theta = 90°$, $\psi_{max} = 0.946$.

constant in this study (i.e. Darcy number is based on κ_1), increase in θ makes κ_2 direction approach x_1 (vertical direction). As understood from the earlier studies [22], if the permeability value in the vertical direction increases, the flow becomes faster and increases the convective transport. This is clearly seen in Fig. 4(c) where $\theta = 90°$ and κ_2 coincides with x_1. As κ_2 is higher than κ_1 in Fig. 4(a)–(c), increase in θ increases the strength of the convection and thus increases the energy transport (Table 1).

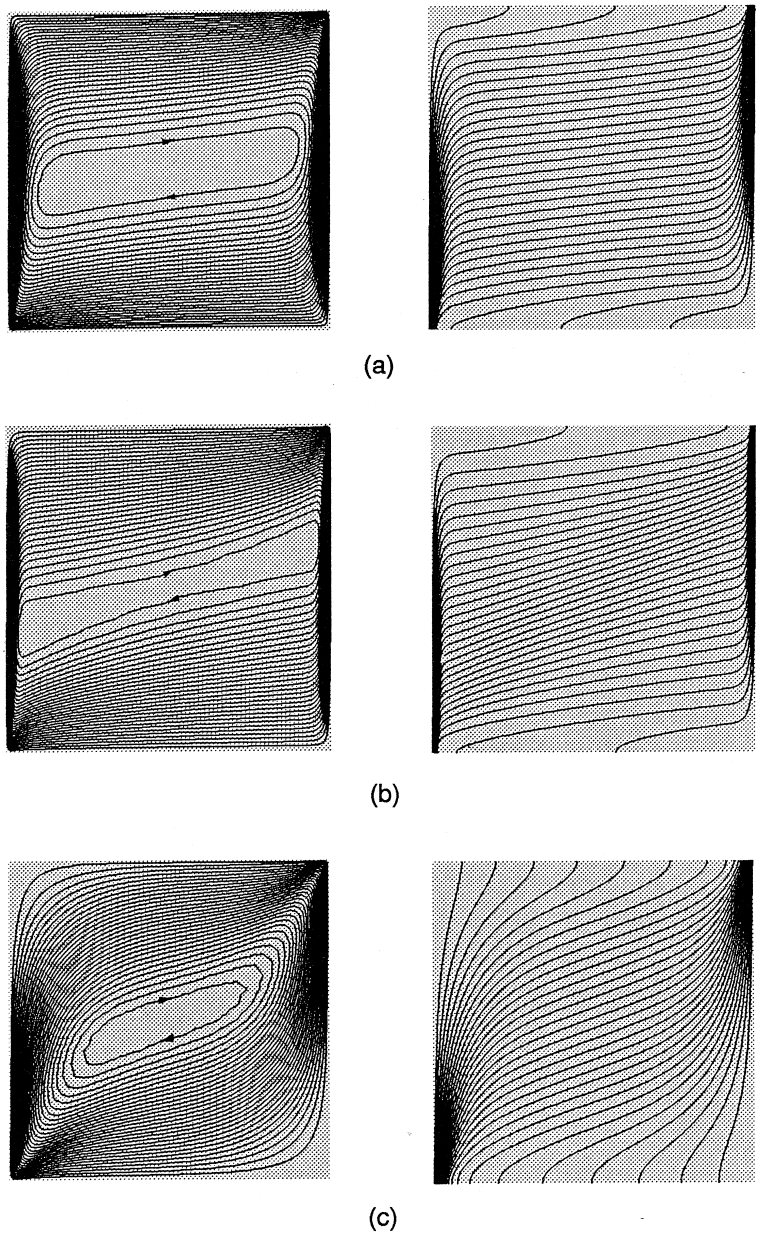

Fig. 6. Flow and isotherm patterns for different θ and permeability ratios in the Darcy flow regime, Da $= 10^{-6}$, Ra $= 10^{9}$, $\epsilon = 0.5$, $k_1^* = 1$, $k_2^* = 1$: (a) $\kappa^* = 0.1$, $\theta = 45°$, $\psi_{\max} = 23.775$; (b) $\kappa^* = 0.1$, $\theta = 90°$, $\psi_{\max} = 38.548$; (c) $\kappa^* = 10$, $\theta = 45°$, $\psi_{\max} = 9.224$.

The reverse of the above discussed process happens when the permeability ratio is higher than unity as shown in Fig. 4(d) and (e). The strength of flow and convection reduces with increase in θ when the permeability value is increased to 10. Also the thermal and flow boundary layers are quite thick here due to higher permeability ratio considered. Here, with increase in θ, the system approaches a diffusion mode where the energy transport is mainly due to conduction.

Almost similar flow properties are observed in the non-Darcy regime (Da $= 10^{-2}$, Fig. 5) except the single phase flow like patterns [28] due to more permeable nature of the medium itself. Also the differences between the isotherm patterns between different parameters are seen to be similar. This is the reason why the average Nusselt numbers are almost the same for different principal permeability directions θ (Table 2).

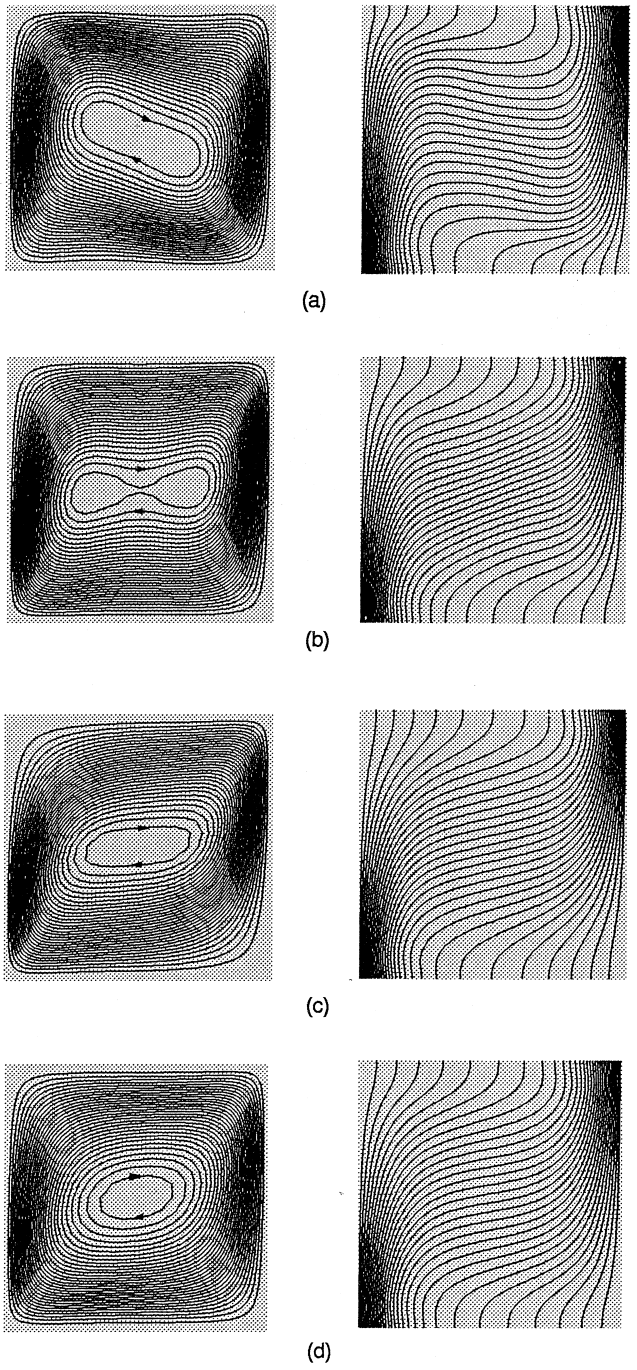

Fig. 7. Flow and isotherm patterns for different θ and permeability ratios in the non-Darcy flow regime, Da $= 10^{-2}$, Ra $= 10^5$, $\epsilon = 0.5, k_1^* = 1, k_2^* = 1$: (a) $\kappa^* = 0.1, \theta = 45°, \psi_{\max} = 7.051$; (b) $\kappa^* = 10, \theta = 0°, \psi_{\max} = 4.618$; (c) $\kappa^* = 10, \theta = 45°, \psi_{\max} = 5.586$; (d) $\kappa^* = 10, \theta = 90°, \psi_{\max} = 4.878$.

Some selected flow and isotherm patterns at higher Rayleigh numbers are given in Figs. 6 and 7 in the Darcy and non-Darcy regimes, respectively. The channeling is increased as the θ value increases in the Darcy flow regime at a lower permeability ratio value ($\kappa^* = 0.1$). However, no channeling is observed in the non-Darcy flow regime (Fig. 7) with change in parameters for the Darcy and Rayleigh number range considered. This can be attributed to the influence of higher non-Darcian forces than that of the Darcy flow

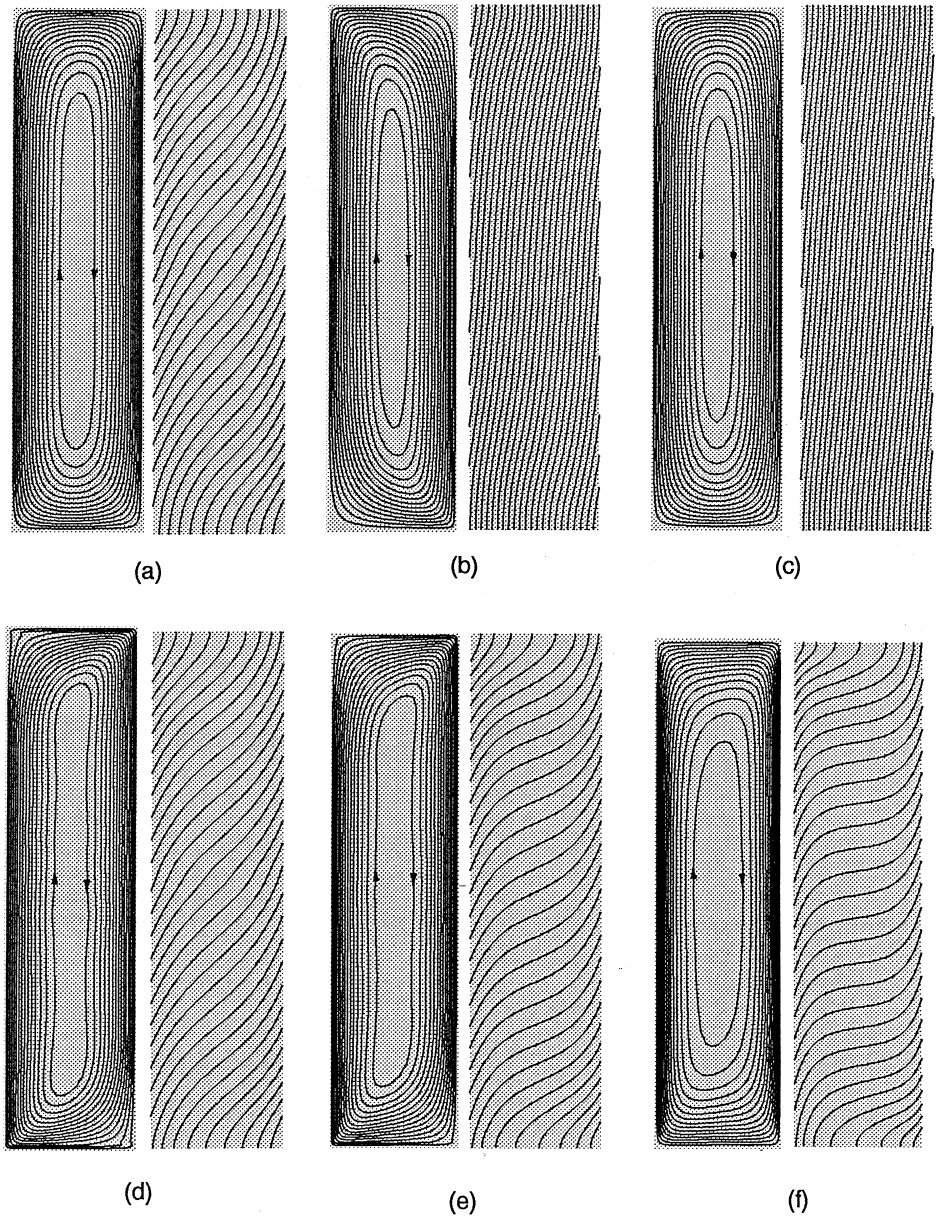

Fig. 8. Flow and isotherm patterns for different θ and permeability ratios, $Ra^* = 20$, $Da = 10^{-6}$, $\epsilon = 0.6$, $A = 4$: (a) $\kappa^* = 10$, $\theta = 0°$, $\psi_c = 1.328$, $T_{max} = 1.177$, $T_{min} = -1.167$; (b) $\kappa^* = 10$, $\theta = 30°$, $\psi_c = 0.725$ $T_{max} = 0.708$, $T_{min} = -0.703$; (c) $\kappa^* = 10$, $\theta = 90°$, $\psi_c = 0.242$, $T_{max} = 0.645$, $T_{min} = -0.645$; (d) $\kappa^* = 0.1$, $\theta = 30°$, $\psi_c = 1.519$, $T_{max} = 1.163$, $T_{min} = -1.173$; (e) $\kappa^* = 0.1$, $\theta = 60°$, $\psi_c = 2.184$, $T_{max} = 1.061$, $T_{min} = -1.067$ (f) $\kappa^* = 0.1$, $\theta = 90°$, $\psi_c = 3.114$, $T_{max} = 0.869$, $T_{min} = -0.873$.

regime. Although significant changes in stream line patterns are observed in the non-Darcy flow regime, only moderate changes are observed in isotherm patterns. In all these patterns discussed above, the Darcy and non-Darcy flow regimes are compared for a given Darcy–Rayleigh number Ra^* ($= Ra\,Da$). This type of comparison brings out all differences between the Darcy and non-Darcy flow regimes.

Above discussed results are for the cavity with vertical walls subjected to isothermal conditions. The second problem considered in this study is a cavity with vertical sides subjected to constant uniform heat flux. It is assumed that heat enters through one vertical side and leaves through the other. A constant temperature is imposed at the cavity center $T = 0$. In this problem the Nusselt number is calculated from the following relation [8]

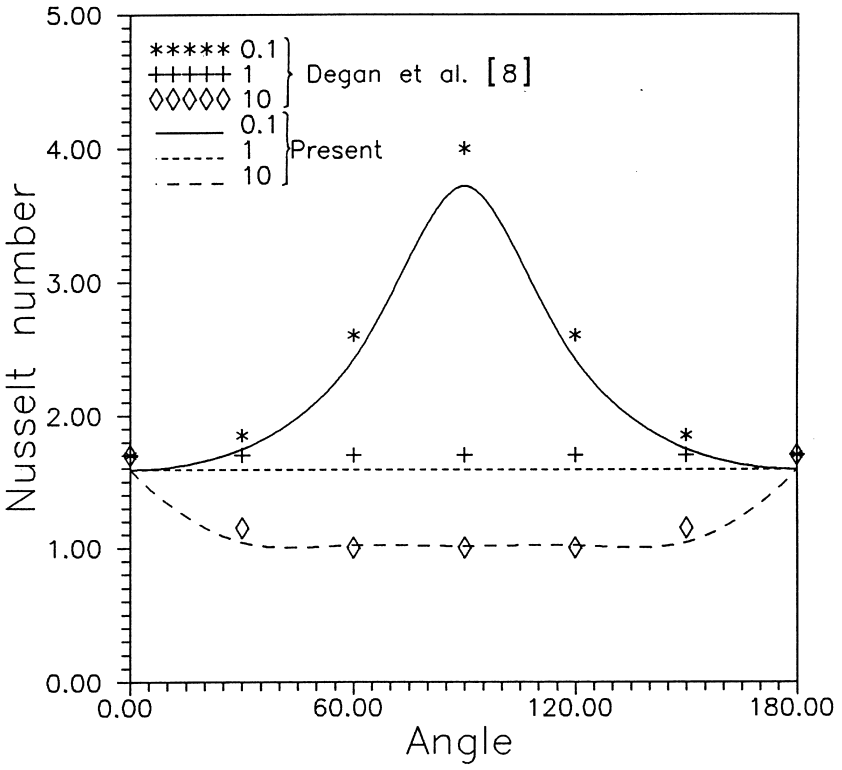

Fig. 9. Average Nusselt number variation with θ for different permeability ratios, Da $= 10^{-6}$, $\epsilon = 0.6$, $A = 4$.

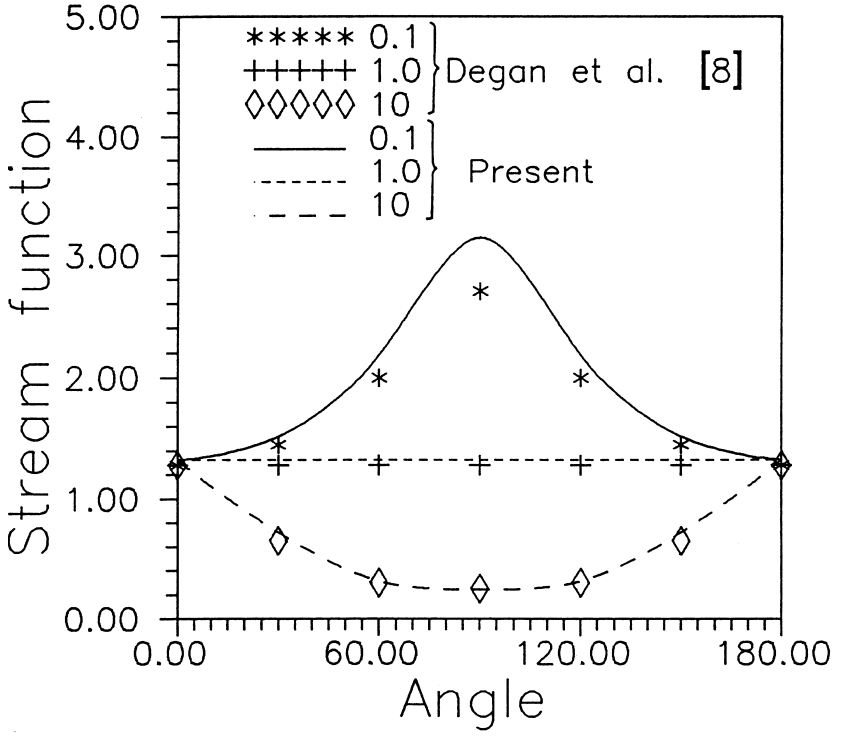

Fig. 10. Variation of stream function at the center of the domain with θ for different permeability ratios, Da $= 10^{-6}$, $\epsilon = 0.6$, $A = 4$.

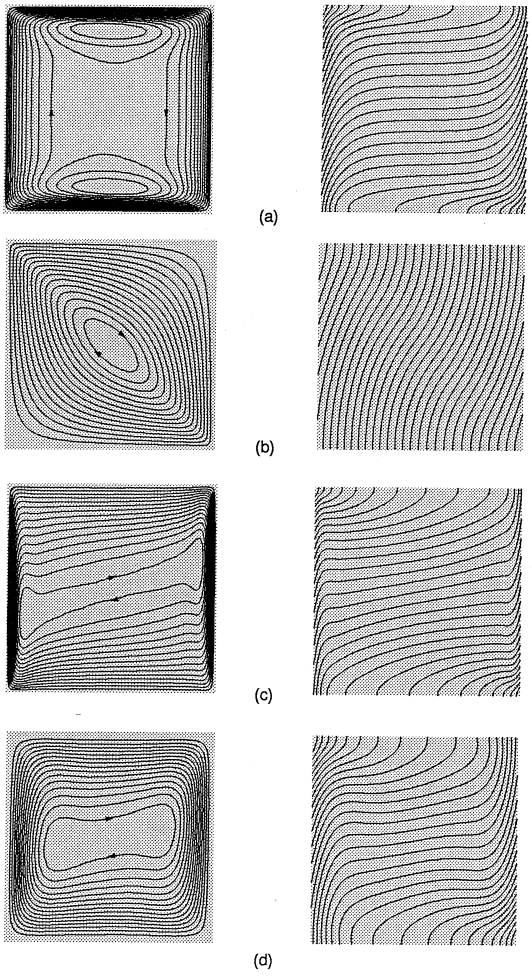

Fig. 11. Flow and isotherm patterns for different Darcy numbers, θ and permeability ratios, $\mathrm{Ra}^* = 500$, $\epsilon = 0.6$, $A = 1$: (a) $\mathrm{Da} = 10^{-5}$, $\kappa^* = 10^{-3}$, $\theta = 0°$, $\psi_{\max} = 4.381$, $T_{\max} = 0.248$, $T_{\min} = -0.248$; (b) $\mathrm{Da} = 10^{-3}$, $\kappa^* = 100$, $\theta = 45°$, $\psi_{\max} = 0.783$, $T_{\max} = 0.570$, $T_{\min} = -0.570$; (c) $\mathrm{Da} = 10^{-5}$, $\kappa^* = 0.01$, $\theta = 90°$, $\psi_{\max} = 5.154$, $T_{\max} = 0.236$, $T_{\min} = -0.236$; (d) $\mathrm{Da} = 10^{-3}$, $\kappa^* = 0.01$, $\theta = 90°$, $\psi_{\max} = 4.118$, $T_{\max} = 0.314$, $T_{\min} = -0.314$.

$$\mathrm{Nu} = \frac{1}{\Delta T}, \tag{19}$$

where ΔT is the temperature difference between the mid-height nodes at the vertical walls.

In Fig. 8, the flow and isotherm patterns are depicted for different permeability ratios and θ at an aspect ratio of 4. These results are in good agreement with those reported in literature [8]. As expected, the isotherms emerge from the side walls due to the heat flux boundary conditions imposed on the vertical walls. As discussed in the previous example, at a higher permeability value, the heat transfer mode approaches conduction with isotherms stand almost vertical (Fig. 8(c)). The reverse happens when the permeability ratios is less than unity. In Figs. 8(d)–(f), the flow and isotherm patterns for a lower permeability ratio (0.1) are presented. Here, as the θ value increases, not only the flow becomes stronger but also the isotherms are stratified with almost zero temperature gradient in the horizontal direction at the middle portion of the cavity. This process where thermal and momentum boundary layers are thin and leads to more energy transfer first along the walls by both convection and diffusion and then to the opposite vertical wall. This type of pattern is often called boundary layer heat transfer regime. On the other hand in Fig. 8(c), the mode is conduction, where the heat transfer is mainly dominated by diffusion rather than convection. This kind of patterns are observed in the earlier example also.

Table 3
Comparison of present predictions with the available results [21], $Ra^* = 500$, $A = 1$, $k^* = 1$

Sl. No.	Da	θ	κ^*	Nu		ψ_{max}		$T_{max} = -T_{min}$	
				Present	Ref. [21]	Present	Ref. [21]	Present	Ref. [21]
1	10^{-5}	0°	10^{-3}	5.66	5.909	4.381	4.40	0.248	0.247
2	10^{-3}	0°	10^{-3}	4.56	4.727	3.968	3.92	0.305	0.3045
3	10^{-5}	45°	10^{2}	1.174	1.173	0.796	0.79	0.569	0.576
4	10^{-3}	45°	10^{2}	1.170	1.170	0.783	0.785	0.570	0.5759
5	10^{-5}	90°	10^{-2}	9.95	10.781	5.154	4.77	0.236	0.2613
6	10^{-3}	90°	10^{-2}	4.729	5.414	4.118	4.175	0.314	0.3041

Fig. 9 shows the Nusselt number variation with θ. As observed in the flow patterns (Fig. 8), the energy transfer is higher with increase in θ at a smaller permeability ratio ($\kappa^* = 0.1$). However, when the permeability ratio is higher than unity, a conduction mode of heat transfer is approached with increase in θ to 90°. At permeability ratio equal to unity, the heat transfer predicted is constant. The comparison with the available results is generally good. However, little difference in agreement can be attributed to the over prediction of the Darcy model used in the referred paper [8]. The corresponding stream function values at the center of the cavity is compared with the available results in Fig. 10.

Fig. 11 shows the flow and isotherm patterns predicted for a cavity with aspect ratio unity and with heat flux boundary conditions. These results are qualitatively in good agreement with the existing Brinkman solution [21]. However, differences do exist in the quantitative results as shown in Table 3. The comparison is generally excellent at higher permeability ratios and smaller θ values. However, the effect of non-linear terms in the present generalised model can be seen from the smaller Nusselt number values predicted at smaller permeability ratios and higher θ values (90°).

5. Conclusions

The natural convection in a hydrodynamically and thermally anisotropic porous medium has been investigated using a simple semi-implicit procedure and the Galerkin finite element method. Two different types of problems have been formulated and solved and the results are discussed in detail. The results show that the present formulation is accurate in predicting the flow and heat transfer. Although the tests have been carried out only for natural convective flows, it is straight forward to use this formulation for forced convective flows.

Further study is essential to understand the usefulness of present formulation for applications such as alloy solidification, flow in heat exchangers etc. Such an analysis will give further insight into the advantages and disadvantages of using the present semi-implicit formulation.

References

[1] S.K. Sinha, T. Sundararajan, V.K. Garg, A variable property analysis of alloy solidification using the anisotropic porous medium approach, Int. J. Heat Mass Transfer 35 (1992) 2865–2877.
[2] A.R. Chaudhuri, K.N. Seetharamu, T. Sundararajan, Modelling of steam surface condenser using finite element method, Comm. Numer. Meth. Engrg. 13 (1997) 909–921.
[3] G. Neale, Degrees of anisotropy for fluid flow and diffusion (electrical conduction) through anisotropic porous media, AIChE J. 23 (1977) 56–62.
[4] O. Kvernvold, P.A. Tyvand, nonlinear thermal convection in anisotropic porous media, J. Fluid Mech. 90 (1979) 609–624.
[5] J. Ni, C. Beckermann, Natural convection in a vertical enclosure filled with anisotropic porous media, ASME J. Heat Transfer 113 (1991) 1033–1037.
[6] W.J. Chang, H.C. Lin, Natural convection in a finite rectangular cavity filled with an anisotropic porous medium, Int. J. Heat Mass Transfer 37 (1994) 303–312.
[7] W.J. Chang, C.F. Haiso, Natural convection in a vertical cylinder filled with anisotropic porous media, Int. J. Heat Mass Transfer 36 (1993) 3361–3367.

[8] G. Degan, P. Vasseur, E. Bilgen, Convective heat transfer in a vertical anisotropic porous layer, Int. J. Heat Mass Transfer 38 (1995) 1975–1987.
[9] J.F. Ephere, Criterion for the appearance of natural convection in an anisotropic layer, Int. Chem. Engrg. 17 615–616.
[10] G. Castinel, M. Combarnous, Natural convection in anisotropic porous layer, Int. Chem. Engrg. 17 (1977) 605–614.
[11] R. McKibbin, P.A. Tyvand, Anisotropic modeling of thermal convection in multilayered porous media, J. Fluid Mech. 118 (1982) 315–339.
[12] K.M. Gjerde, P.A. Tyvand, Thermal convection in a porous medium with continuous periodic stratification, Int. J. Heat Mass transfer 27 (1984) 2289–2295.
[13] T. Nilsen, L. Storesletten, An analytical study on natural convection in isotropic and anisotropic porous channels, ASME J. Heat Transfer 112 (1990) 396–401.
[14] K. Vafai, C.L. Tien, Boundary and inertia effects on flow and heat transfer in porous media, Int. J. Heat Mass Transfer 24 (1981) 195–203.
[15] K. Vafai, C.L. Tien, Boundary and inertia effects on convective mass transfer in porous media, Int. J. Heat Mass transfer 25 (1982) 1183–1190.
[16] P. Nithiarasu, K.N. Seetharamu, T. Sundararajan, Natural Convective heat transfer in an enclosure filled with fluid saturated variable porosity medium, Int. J Heat Mass Transfer 40 (16) (1997) 3955–3967.
[17] P. Nithiarasu, K. Ravindran, A new semi-implicit scheme for buoyancy driven flow in a fluid saturated porous medium, Comp. Meth. Appl. Mech. Engrg. 165 (1998) 147–154.
[18] P. Nithiarasu, K.N. Seetharamu, T. Sundararajan, Double-diffusive natural convection in an enclosure filled with fluid saturated porous medium – A generalised non-Darcy approach, Numer. Heat Transfer, Part A 30 (1996) 413–426.
[19] P. Nithiarasu, K.N. Seetharamu, T. Sundararajan, Numerical prediction of buoyancy driven flow in fluid saturated non-darcian porous medium, Int. J. Heat Mass Transfer 42 (1999) 1205–1215.
[20] P. Nithiarasu, K.N. Seetharamu, T. Sundararajan, Non-Darcy Double-Diffusive Convection in fluid saturated axisymmetric porous cavities, Heat and Mass Transfer 36 (1997) 427–434.
[21] G. Degan, P. Vasseur, Boundary – layer regime in a vertical porous layer with anisotropic permeability and boundary effects, Int. J. Heat Fluid Flow 18 (1997) 334–343.
[22] P. Nithiarasu, K.N. Seetharamu, T. Sundararajan, Heat and mass transfer in a fluid saturated anisotropic porous medium, in: Third ISHMT and ASME conference and 14th National Heat and Mass Transfer Conference, IIT Kanpur, 1997, pp. 661–666.
[23] P. Nithiarasu, K.S. Sujatha, K.N. Seetharamu, T. Sundararajan, Buoyancy driven flow in a non-Darcian fluid saturated porous enclosure subjected to uniform heat flux – A numerical study, Comm. Numer. Meth. Engrg., in press.
[24] S. Ergun, Fluid Flow through packed column, Chem. Engrg. Progress 48 (1952) 89–94.
[25] A.J. Chorin, Numerical solution of Navier Stokes equations, Math. Comp. 22 (1968) 745–762.
[26] B. Ramaswamy, T.C. Jue, J.E. Akin, Semi-implicit and explicit finite element schemes for coupled fluid/thermal problems, Int. J. Numer. Meth. Engrg. 34 (1992) 675–696.
[27] P. Nithiarasu, K.N. Seetharamu, T. Sundararajan, Finite element analysis of transient natural convection in an odd-shapped enclosure, Int. J. Numer. Meth. Heat Fluid Flow 8 (1998) 199–216.
[28] N. Massaroatti, P. Nithiarasu, O.C. Zienkiewicz, Characteristic – Based – Split (CPS) Algorithm for Incompressible Flow Problems with Heat Transfer, Int. J. Numer. Meth. Heat Fluid Flow 8 (1998) 969–990.
[29] K.L. Walker, G.M. Homsy, Convection in porous cavity, J. Fluid Mech. 87 (1978) 449–474.